Tellus (1997), 49A, 595–612
Printed in UK – all rights reserved

TELLUS
ISSN 0280–6495

Numerical simulation of the Valentine's day storm during the 1990 winter icing and storms project

By P. A. HAINES[1]*, *Department of Meteorology, Arrhenius Laboratory, Stockholm University, S-106 91 Stockholm, Sweden,* and J.-D. CHERN AND W.-Y. SUN, *Department of Earth & Atmospheric Science, Purdue University, West Lafayette, Indiana 47907, USA*

(Manuscript received 21 April 1995; in final form 11 August 1997)

ABSTRACT

This paper discusses numerical simulation of the first day of the 1990 winter icing and storms project's (WISP) Valentine's day storm (VDS) case with the Purdue mesoscale model (PMM) and comparison of the results to aircraft, satellite, radiometer and other observations. This situation is marked by many observations of supercooled liquid water (SLW) contents of 0.2 g m^{-3} to 0.3 g m^{-3} by the WISP research aircraft. The PMM was initialized with the ECMWF analysis for 13 February 1990 at 0000 GMT and used to make an 18-h forecast with output every 6 h. This paper focuses on comparison of the forecast to observations made at about 1800 GMT since the aircraft encountered significant amounts of SLW during its flight between 1723 GMT and 1928 GMT. Dual channel radiometer, satellite visible imagery, and other observational data sources are also utilized. For this study, the PMM includes a new stable cloud parameterization that is discussed here. In it, cloud water and ice are explicitly calculated while rain and snow are implicitly handled. Between 0 and -40°C, cloud water and cloud ice can coexist; the conversion of cloud water to cloud ice is governed by the depositional growth rate of ice crystals whose concentration is diagnosed on the basis of temperature. After accounting for precipitation, a saturation adjustment is done to remove either supersaturated vapor or subsaturation in the presence of cloud drops. In mixed phase conditions, both saturation vapor pressure and the apportionment of condensate into ice or liquid are on a mass-weighted basis according to the existing amounts of ice and liquid or on the basis of temperature if there is neither.

1. Introduction

Forecasts of aircraft icing, clear air turbulence, and other weather hazardous to aviation are issued by the Aviation Weather Center (AWC) in Kansas City. In making their forecasts, AWC relies heavily upon numerical model guidance provided by the National Center for Environmental Prediction (NCEP), although processing of gridded numerical model output is done at AWC. Cloud water mixing ratios are now available from the eta model; however, their evaluation and possible use in making aircraft icing forecasts remains to be completed (Tansey and McCann, 1997). The stable cloud parameterization currently used in the eta model (Zhao, 1994) represents restrictions that are necessary in the face of operational computational capabilities. As these restrictions are relaxed, it will be possible to apply a more complete cloud parameterization along the lines of that discussed and tested here.

Aircraft icing forecasts continue to be too imprecise to provide pilots with knowledge of impending icing conditions (Federal Coordinator for

[1] Corresponding author.
* Present affiliation: Army Research Laboratory, White Sands Missile Range, NM 88002, USA.

Meteorological Services and Supporting Research, 1986; Rasmussen et al., 1992), and due to forecast inaccuracies, the general tendency is to overpredict the extent and the severity of icing. Since a forecast of icing curtails or prevents the operation of an aircraft not certified or equipped for flight in such conditions, more accurate icing forecasting will allow many aircraft to fly that must now remain on the ground. The flight planning and scheduling of the transport aircraft system would also benefit greatly from such forecasts.

Ideally, an aircraft icing forecast would be based on gridded prognoses of cloud liquid water amount, its drop-size distribution, and temperature, but even having the cloud water amounts and temperatures would be of great benefit. Recent simulations by mesoscale models have demonstrated their capability to successfully capture the dynamical evolution of a number of different events (Sun et al., 1991; Kuo et al., 1992; Sundqvist et al., 1989; Zhang and Gao, 1989) and the dynamics and initialization of these models continue to be improved. Meanwhile, their treatment of cloud processes needs to be evaluated and improved in order to enable much better prediction of quantitative precipitation, cloud cover, and aircraft icing. The aircraft and other observations that have been made during the 1990 WISP program provide an excellent opportunity with which to do this.

In this study, we have applied the PMM with a detailed microphysical parameterization to the VDS case observed during the WISP program to evaluate both its forecast and its cloud parameterization. Recently, Modica et al. (1994) used the MM4 model in simulating the VDS; however, many more comparisons between the simulated and observed microphysical fields of this and other situations need to be done. The VDS case is interesting for several reasons. During 13 February, quite extensive aircraft and other observations were made with which to evaluate the model and parameterization. In addition, precipitation was generally light over eastern Colorado making it easier to evaluate the process of cloud glaciation in the model. Finally, this case has been studied by other investigators (Rasmussen et al., 1995) so there are analyses and results with which to evaluate and compare our results.

As mentioned, the model used is the PMM, which has been successfully applied to a wide variety of mesoscale phenomena. Both the model and the microphysical parameterization are described in Section 2. The data used and initialization of the PMM along with a brief description of the VDS weather situation are covered in Section 3. The results are presented and discussed in Section 4. Finally, the conclusions of this work along with plans for future work are given in Section 5.

2. Numerical model

More complete details about the PMM and some of its results are available in Sun et al. (1991), Sun and Chern (1993), and Sun and Chern (1994). The PMM is a hydrostatic model employing the sigma-p coordinate in the vertical and includes detailed parameterizations of shortwave and longwave radiation for both cloudy (with liquid water) and clear skies, budget equations for surface moisture and heat fluxes, and a turbulence parameterization with explicit calculation of the turbulent kinetic energy. Detailed descriptions of these parameterizations are available in Sun and Wu (1992), Wu and Sun (1990), and Sun (1993a,b). The integration of the governing equations is split into three time steps. A small time interval with a forward-backward scheme (Sun, 1980, 1984) is used for inertia-gravity wave terms. The longer time step that is limited by horizontal advection, is applied to horizontal advection, phase changes of water substance, diffusion terms, and the surface budget equations. A very long time interval of about ten minutes is used in calculating the radiation parameterization.

As used here, the model has 60 vertical layers in a stretched grid extending from the surface up to 100 mb. The finest vertical spacing of just over 100 meters, is in proximity to the ground in order to better treat surface vertical moisture and heat fluxes. The interior grid domain covers an area of about 800 000 km^2 with 50 grid points in the west to east direction and 40 grid points in the south to north direction and a horizontal grid spacing of 20 km. The interior grid is surrounded by a buffer zone with a 6 Δx space interval to avoid reflection and other possible deleterious effects associated with the time-dependent lateral boundary. Newtonian damping is applied to the top 5 levels to avoid reflection of gravity waves from the top. Horizontal smoothing is also applied in order to prevent nonlinear instability.

Currently, equivalent ice potential temperature, θ_{ei}, the horizontal wind components, u and v, the total water mixing ratio, q_w, cloud water amount, q_l, and cloud ice amount, q_i, are explicitly predicted while temperature, T, rain, q_r, and snow, q_s, are diagnosed. Here θ_{ei} is defined as,

$$\theta_{ei}=\theta+\theta/T(L_v q_v/c_p+L_s q_i/c_p),$$

where L_v is the latent heat of vaporization, q_v is the water vapor mixing ratio, L_s is the latent heat of sublimation, and c_p is the specific heat at constant pressure. It should be noted that θ_{ei} is defined differently here than in Tripoli and Cotton (1981). The saturation temperature and saturation mixing ratio are extracted iteratively from θ_{ei} and q_w.

The microphysical parameterization used here follows Lin et al. (1983) and Rutledge and Hobbs (1983; 1984), and the various snow and rain production and depletion processes are named and defined as in Lin et al. It contains four classes of hydrometeors: cloud water, cloud ice, rain, and snow in which cloud water and cloud ice are explicitly predicted, but snow and rain are implicitly handled. In the absence of turbulent mixing and precipitation or evaporation, the total water, q_w, is conserved. Total water is expressed as

$$q_w=q_l+q_i+q_v, \quad (1)$$

where q_l, q_i, and q_v are, respectively, the mixing ratios of cloud water, cloud ice, and water vapor. Snow is generated by collision and aggregation of smaller cloud ice particles, contact freezing of small raindrops, depositional growth, and riming of ice crystals. It is depleted by melting and sublimation. The total production rate for snow is

$$P_S=P_{SAUT}+P_{SFW}+P_{SFI}+P_{SACI}+P_{SACW}+P_{RACI}+P_{IACR}+P_{SACR}+P_{SDEP}+P_{SSUB}, \text{ for } T<0°\text{C},$$

or

$$P_S=P_{SMLT}+P_{SMLTEVP} \quad \text{for } T\geqslant 0°\text{C}, \quad (2)$$

where P_{SAUT} is the rate of autoconversion from cloud ice to snow, P_{SFW} is the rate of snow production from cloud water to snow by the Bergeron process, P_{SFI} is the rate of snow production from cloud ice by the Bergeron process, P_{SACI} is the rate of snow production by accretion of cloud ice, P_{SACW} is the rate of snow production by accretion of cloud water, P_{RACI} is the rate of snow formation from rain that freezes when impacted by cloud ice, P_{IACR} is the rate of snow formation from cloud ice when it impacts and freezes rain, P_{SACR} is the rate of snow production by accretion of rain, P_{SDEP}/P_{SSUB} is the rate of snow production/depletion from depositional growth/sublimation, P_{SMLT} is the rate at which snow melts, and $P_{SMLTEVP}$ is the rate of evaporation of melting snow. It should be noted that all production and depletion processes are defined as in Lin et al.

Rain is generated by collision and coalescence of cloud droplets, accretion of cloud water, accretion of cloud water by snow at above freezing temperatures, and melting of snow. It is depleted when frozen by contact with cloud ice particles, accretion by snow, and evaporation. The total production rate of rain is,

$$P_R=P_{RAUT}+P_{RACW}-P_{IACR}-P_{SACR}+P_{REVP} \quad \text{for } T<0°\text{C},$$

$$P_R=P_{RAUT}+P_{RACW}+P_{SACW}-P_{SMLT}+P_{REVP} \quad \text{for } T\geqslant 0°\text{C}, \quad (3)$$

where P_{RAUT} is the rate of rain production from autoconversion of cloud water, P_{RACW} is the rate of rain formation by accretion of cloud water, and P_{REVP} is the rate of rain depletion from evaporation of rain. At above freezing temperatures, the accretion of cloud water by snow is assumed to produce rain drops, P_{SACW}, and all other processes are defined as above.

In order to avoid the small time steps necessary to prevent numerical instability when precipitation fall speeds are large, precipitation is predicted implicitly; that is, the mixing ratios of rain and snow are calculated diagnostically so that the various production terms mentioned above may be calculated. Following Nagata and Ogura (1991), precipitation is allowed to fall and interact with other hydrometeors layer by layer until it either reaches the ground or completely evaporates or sublimates. At each time step, the downward flux of rain or snow (f_{rk} or f_{sk}) at the top of each layer is assumed constant and no rain or snow remains in the air at the end of a time step. The downward fluxes of rain and snow are given respectively by

$$f_{rk}=(\rho q_r U_R)_k=\sum_{k'=1}^{k-1}(P_R \Delta p/g)_{k'}, \tag{4}$$

$$f_{sk}=(\rho q_s U_S)_k=\sum_{k'=1}^{k-1}(P_S \Delta p/g)_{k'}, \tag{5}$$

where Δp_k is the thickness of the kth layer measured in pressure and U_S and U_R are the mass-weighted mean terminal velocities of respectively snow and rain. Note that the k' index above increases downward beginning from 1 at the top layer. In each layer, the precipitation mixing ratios are diagnosed from the downward fluxes and terminal velocities.

The microphysical production terms in the prognostic equations for cloud water, q_l, and cloud ice, q_i, are

$$\begin{aligned} dq_l/dt &= -P_{RAUT}-P_{SACW}-P_{SFW}-P_{RACW} \\ &\quad -P_{IHOM}-P_{IDW}, \text{ for } T<0°C, \\ dq_l/dt &= -P_{RAUT}-P_{SACW}-P_{RACW}+P_{IMLT}, \\ &\quad \text{for } T\geqslant 0°C, \\ dq_i/dt &= -P_{SAUT}-P_{SACI}-P_{SFI}-P_{RACI} \\ &\quad +P_{IHOM}+P_{IDW}, \text{ for } T<0°C, \\ dq_i/dt &= -P_{IMLT}, \text{ for } T\geqslant 0°C \end{aligned} \tag{6}$$

The rates of conversion between cloud liquid and cloud ice in mixed phase clouds are of particular interest and importance to the aircraft icing problem. Large amounts of SLW are usually precluded by precipitation. In the absence of precipitation, at temperatures below 0°C, an important depletor of SLW is cloud glaciation. At temperatures below −40°C, all existing cloud water is frozen to cloud ice; this is accounted for by the P_{IHOM} term above. For temperatures above 0°C, all cloud ice melts to form cloud water as accounted for by the P_{IMLT} term. Between 0°C and −40°C, cloud water and cloud ice can coexist, however, the lower saturation vapor pressure over ice favors conversion of the water to ice. The rate at which this occurs is governed by the depositional growth rate of ice crystals (Koenig, 1971; Hsie et al., 1980),

$$P_{IDW}=N_u(a_1 m_n^{a_2})/\rho, \tag{7}$$

where m_n is the assumed mass of a growing ice crystal, 10^{-12} g, N_u is the number concentration of active ice nuclei, and a_1 and a_2 are temperature dependent parameters. The depositional growth rate is a well-established microphysical process if the number of growing ice crystals, N_u, is known. Measurements show that N_u and the number of growing ice crystals can differ by up to an order of magnitude (Rasmussen, personal communication, 1994), but understanding of why this is so and methods to account for the discrepancy in numbers are not yet available. Currently, N_u is given by the temperature dependent diagnostic relation originated by Fletcher (1962),

$$N_u=n_0 \exp(\beta_1 \Delta T), \tag{8}$$

where ΔT is the supercooling in degrees Kelvin and n_0 and β_1 are respectively 0.01 m^{-3} and 0.5. The microphysical production or depletion of total water, q_w, is

$$dq_w/dt=-P_r-P_s,$$

or

$$\begin{aligned} dq_w/dt &= -P_{RAUT}-P_{SACW}-P_{SFWI}-P_{RACW} \\ &\quad -P_{SAUT}-P_{SFI}-P_{SACI}-P_{REVP} \\ &\quad -P_{RACI}-P_{SDEP}-P_{SSUB}, \text{ for } T<0°C, \\ dq_w/dt &= -P_{SMLTEVP}-P_{REVP}-P_{RAUT} \\ &\quad -P_{RACW}-P_{SACW}, \text{ for } T\geqslant 0°C, \end{aligned} \tag{9}$$

where all production processes are defined as above.

After accounting for the various precipitation productions, a saturation adjustment scheme is applied in order to remove any supersaturated vapor or subsaturation in the presence of cloud drops. This is done iteratively by the Newton-Raphson method to balance the heat exchange and change of water phase. It is assumed that the ice equivalent potential temperature, the total water, and the mass ratio of cloud water and cloud ice are fixed during the adjustment.

A related question is what to do when supersaturation first occurs at temperatures below 0°C. What is the appropriate saturation vapor pressure and how much of the condensate/sublimate becomes ice and how much becomes water? Matveev (1984) reported the statistics of occurrence of liquid, mixed phase, and ice clouds as a function of temperature for over 60 000 aircraft observations made in more than 40 000 clouds. Sundqvist (1993) utilized these statistics to construct two frequency distributions as a function of temperature. The first is for pure ice clouds and the second is for ice and mixed phase clouds together. It seems that some combination of these curves can be an indication of the relative proportion of ice as a function of temperature.

To roughly average both curves together, we use a linear function of ambient temperature to govern the proportion of condensate that is sublimated. None is sublimated for temperatures above −5°C and all is sublimated for temperatures below −25°C. Between these two temperatures, the proportion sublimated is a linear function of temperature going from 0 at −5°C to 1 at −25°C. That part of the condensate not sublimated is condensed. Similarly, the saturation vapor pressure is a weighted average of that over water and that over ice. At temperatures above −5°C, only the saturation vapor pressure over water is used; below −25°C, only the saturation vapor pressure over ice is used. Between −5°C and −25°C, there is a mixed weighting of saturation vapor pressures over ice and over water in which the weighting of the ice saturation vapor pressure goes from 0 at −5°C to 1 at −25°C with the water saturation vapor pressure weighted inversely.

With cloud present, the percent of supersaturated water vapor that is sublimated is according to the percent of condensate constituted by ice at the start of the time step. The remainder becomes cloud water. The saturation vapor pressure is treated in a similar manner consisting of a mass-weighted mean of the saturation vapor pressures over ice and water according to the relative masses of these constituents at the beginning of a time step.

In summary, a mass-weighted saturation adjustment scheme similar to Tao et al. (1989) and Lord et al. (1984) but utilizing Sundqvist (1993) is used. For supersaturation in clouds, the resulting condensate is partitioned into cloud water or ice according to this mass-weighting. A key assumption is the initial amount of cloud ice and water for temperatures between −0° and −40°C. Thereafter, the amount of ice and water is free to vary following the depositional growth rate of ice crystals at the expense of cloud water.

3. Data and model initialization

The model was initialized with the ECMWF analysis for 0000 GMT on February 13, 1990 as interpolated to the model grid and domain used here. A Lambert conformal projection was used. The grid domain encompasses Colorado and includes the southern half of Wyoming, western Nebraska and small parts of adjacent Kansas, Utah, Oklahoma, New Mexico, and Arizona, and it is centered on the Denver-Stapelton airport. The grid domain extends vertically from the surface to the 100 mb surface, and with 60 points in that direction, the average grid spacing is about 200 m. As mentioned, a time dependent lateral boundary condition is employed. Conditions on the lateral boundary at any given time were obtained by linearly interpolating in time the bracketing ECMWF analyses that are available every six hours. No other preparation of initial conditions was done for the PMM.

This particular case was a well observed event during the 1990 phase of WISP. WISP is being conducted in eastern Colorado to study and increase the understanding of the dynamics and microphysics associated with the formation and depletion of SLW in winter storms, and to improve the forecasting of aircraft icing. As shown in Fig. 1, during 1990, WISP included special data collection by Doppler radars, aircraft, radiometers, mesonet stations, and the Cross-Chain Loran Atmospheric Sounding System (CLASS) as well as regular data collection by wind profilers, rawinsonde observations, and visible and infrared satellite imagery (Rasmussen et al., 1992). There have been three major and one minor WISP observing programs during the winters of 1990, 1991, and 1994 that have included several significant cases in which widespread occurrence of SLW caused moderate to severe aircraft icing. During the 1990 VDS, a considerable amount of SLW observations were made by both research aircraft and microwave radiometers.

The VDS extends from 0000 GMT on 13 February through 15 February 1990, during which a persistent low level upslope flow over eastern Colorado caused a notable period of SLW occurrence there. This episode was extensively observed by the WISP network with numerous research aircraft observations (Rasmussen et al., 1992), and was marked by a number of pilot reports of aircraft icing. After 0000 GMT on 13 February, following the passage of the first cold front, a shallow high pressure dome developed over Nebraska and Kansas. Later, at about 1400

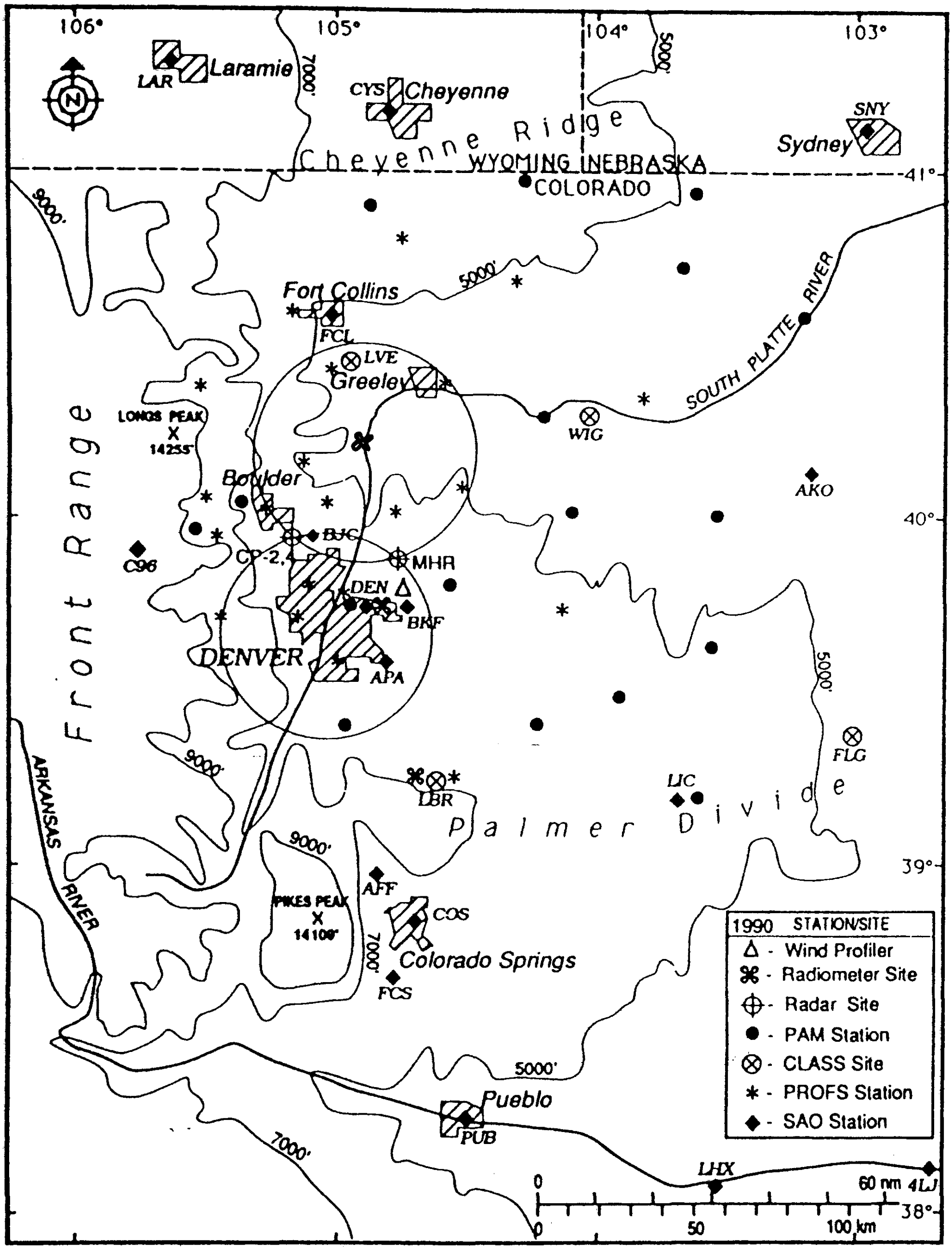

Fig. 1. WISP 90 observing network with dual-Doppler lobes and topographic contours at every 2000 ft. (after Rasmussen et al., 1992).

GMT on February 13, a secondary surge of arctic air passed through northeastern Colorado before stalling at the Palmer divide for the next 6 to 12 h (Rasmussen et al., 1992). As a result of the cold fronts, temperatures in eastern Colorado plummeted from 15° to 20°C on 12 February to nearly −20°C on the morning of 15 February. After 0900 GMT on 13 February, the shallow upslope flow in eastern Colorado was topped by a cloud layer several hundred meters thick that contained widespread SLW in excess of 0.2 gm m^{-3} with pockets up to 0.5 gm m^{-3}. Until 15 February, this cloud layer continued to be shallow and confined beneath a strong inversion that was topped by a very dry southwesterly flow; hence, precipitation was generally light. On 15 February, upper air support improved due to a trough approaching from the west resulting in deeper overturning, thicker cloud layer(s), and more significant precipitation in the WISP observation region. From 13 to 15 February, the cloud temperatures generally decreased with time as colder air invaded the region with a consequent increase in the likelihood of cloud glaciation. In this study, attention is focused on the earliest part of the period during 13 February when most of the SLW occurred, there were numerous SLW observations, and, as mentioned, precipitation was sparse.

Beginning at 0000 GMT on 13 February, the PMM was run to produce an 18 hour forecast of the conditions over eastern Colorado and vicinity with output available every six hours.

4. Results and discussion

Few detailed comparisons have been done of microphysical predictions by a mesoscale model to aircraft and other observations; an example is Modica et al. (1994). Before examining the results, a few remarks on the limitations of this kind of procedure seem warranted. Both the dynamics and microphysics of a given situation can and likely will contribute to discrepancies in the comparisons. Therefore, we believe, it is prudent to first examine the comparison between model predictions and observations to evaluate the model's capability to produce dynamically similar results. This will be useful later when comparing the predicted cloud amounts to the observations since, at minimum, we have established the importance of or have absolved the dynamics from causing discrepancies in the comparisons. The movement and intensity of the cold fronts, their interaction with the underlying terrain and overlying flow, and the development of a synoptic scale upslope flow are the most important dynamical aspects of this case. In order to evaluate the model's predictions of these, we utilize both the CLASS soundings and surface mesonet observations. In addition, we compare a composite of the cloud cover predicted by the model at 1800 GMT to visible satellite imagery made at 1700 GMT on 13 February 1990. These comparisons demonstrate that the PMM simulates the dynamical forcings of this case reasonably well and that the model's overall prediction of the horizontal distribution and coverage of cloud cover is comparable to that observed. In addition, precipitation was sparse and light during February 13 allowing these comparisons to more narrowly focus on cloud formation and glaciation by the model.

With the model's capability for treating the dynamics of this case established, we move on to microphysical comparisons between the model and aircraft observations. In particular, we focus on a south to north ($y-z$) cross-section that was well observed by the aircraft during a two hour period from 1723 to 1928 GMT on 13 February 1990. The cloud liquid water content, temperature, and winds calculated by the model are examined and compared to the observations there.

In order to augment and extend the aircraft observations, we include comparisons with the dual-channel radiometers as well as pilot reports of aircraft icing. These comparisons provide additional evidence in support of the model's capability for predicting the amount and location of the cloud during this case. The pilot reports of icing during 13 February are also considered; they are additional evidence since some are located where neither the research aircraft nor by the radiometers made observations.

4.1. *Class and mesonet comparisons*

Fig. 2 shows the comparison between the Loveland CLASS rawinsonde observation of winds, temperature, and dewpoint made at 1800 GMT on 13 February 1990 and the PMM forecasts of same. Both the observations and the

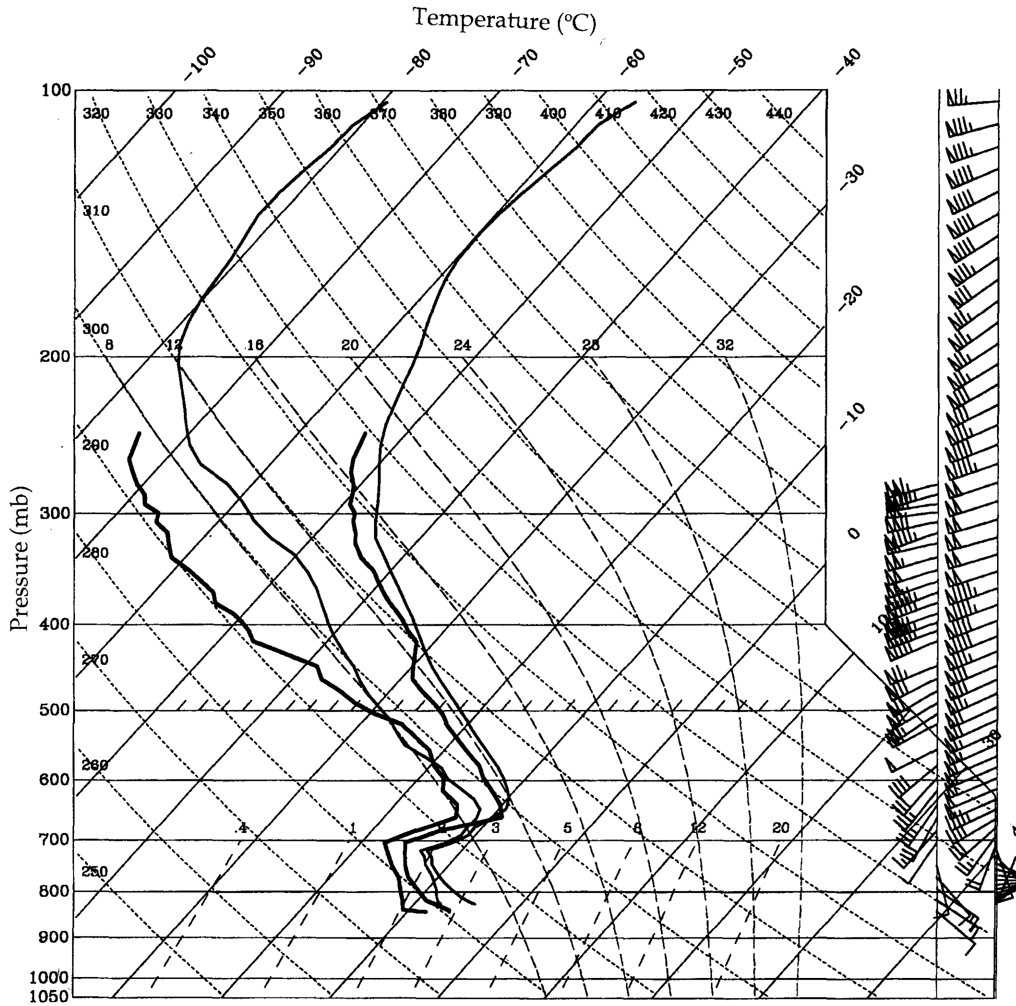

Fig. 2. Comparison of Loveland CLASS rawinsonde sounding at 1800 GMT on 13 February 1990 to the PMM forecast sounding for the same place and time. The CLASS temperature and mixing ratios are shown by the dark solid lines while those forecast by the PMM are shown by the light solid lines. On the far right side of the figure, the PMM forecast winds appear to the right of the CLASS observed winds.

model show that the cold air layer near the ground is capped by a strong inversion that extends up to about 650 mb. The cold layer is quite humid and largely occupied by cloud cover as shown by aircraft observations at this time. Near the ground, the PMM temperature is about 2°C warmer than observed, but in the upper half of the cloud layer its temperature is nearly the same as the observation. Above the top of the cloud and inversion, the model temperatures are about 2°C degrees warmer than observed; however, the temperature comparisons at the other CLASS locations are in much closer agreement. Above the inversion, the observed dewpoints decrease quite rapidly with height and it is very dry in the middle and upper troposphere. Rasmussen et al. (1995) attribute this drying to subsidence induced as a jet streak propagated into the Colorado region. The model also shows drying but not as pronounced as was observed. Along the right side of Fig. 2 are observed and modeled profiles of horizontal winds respectively. Both in speed and direction, the model winds are in good agreement with those observed.

Fig. 3 shows the same kind of comparison as Fig. 2 except that it is for Flagler at 0000 GMT on 14 February 1990. This comparison is much the same as for Fig. 2 except that the model and observed temperatures above the cloud layer are in quite close agreement and that the model winds near the ground are somewhat stronger than observed. The comparisons shown in Figs. 2 and 3 are generally representative of those on 13 February.

To further corroborate the model's capability to capture the dynamics of this case, we present two comparisons of the modeled and observed surface wind fields at 1500 GMT and 1800 GMT on 13 February 1990. A Denver Cyclone (DC) circulation (Szoke et al., 1984) developed in this time period. The observed fields are based on analysis of the WISP mesonet and show at 1500 GMT (Fig. 4) that the surface flow was generally easterly at 5 to 10 m s^{-1}. Fig. 5 shows the corresponding surface wind field predicted by the model which is in good agreement with the observations.

By 1800 GMT, the observed surface flow (Fig. 6) shows a very distinct DC circulation centered about 50 km south and slightly to the east of the mile high radar (MHR) location. This circula-

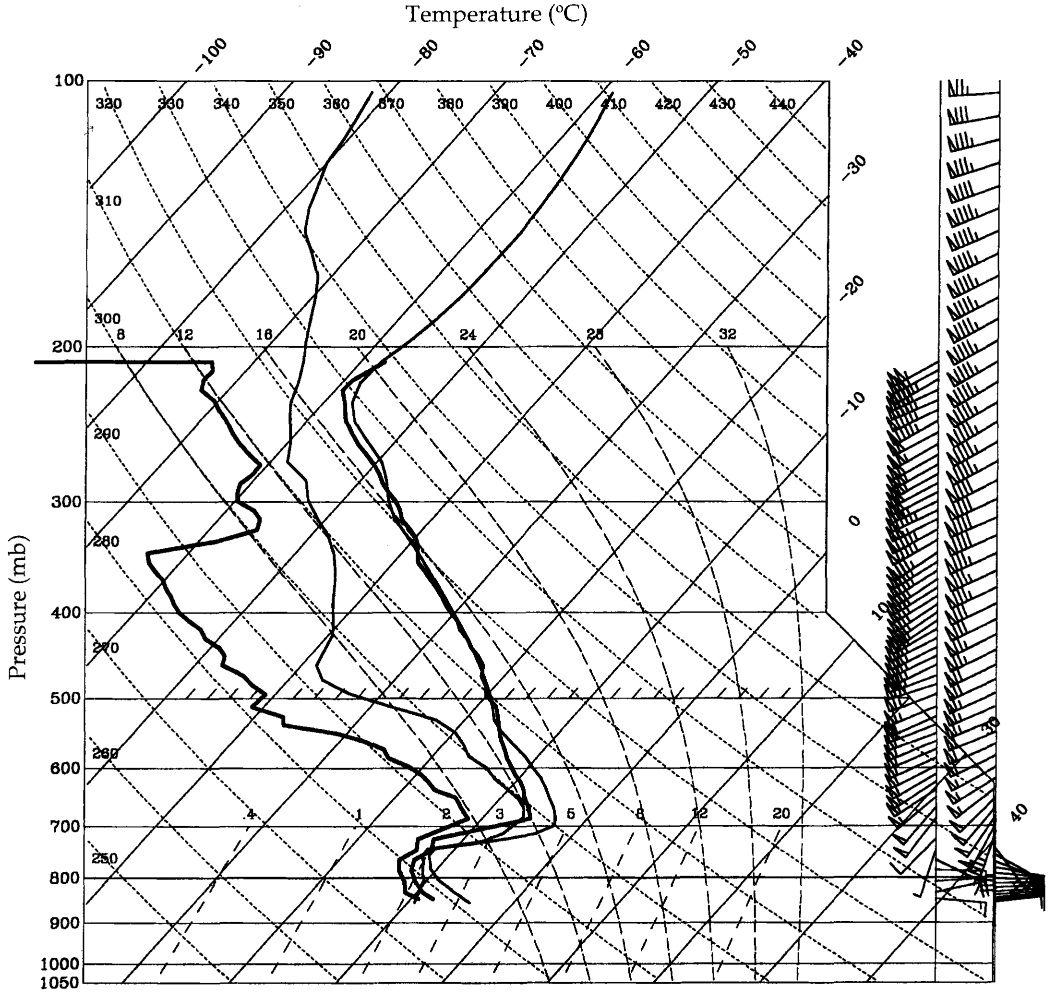

Fig. 3. As for Fig. 2, but for Flagler at 0000 GMT on 14 February 1990.

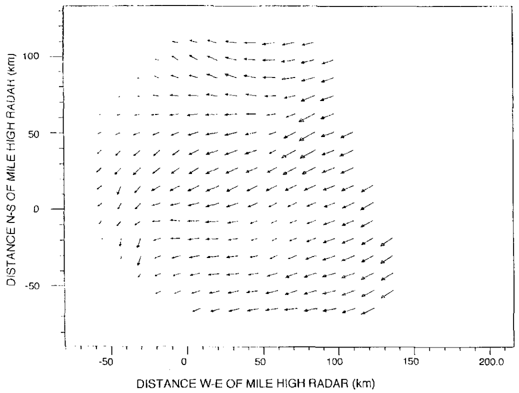

Fig. 4. Gridded analysis of mesonet winds at 1500 GMT on 13 February 1990. The wind vector scale is shown below the figure.

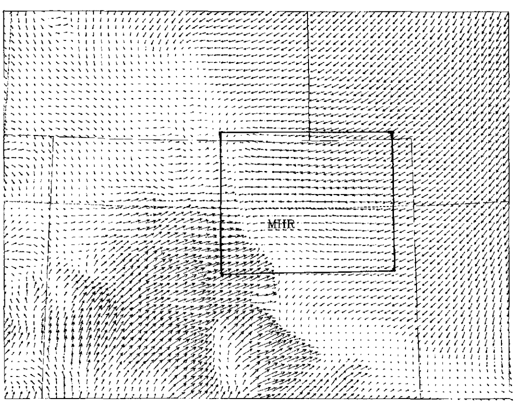

Fig. 5. PMM 15-h forecast of surface winds valid for 1500 GMT on 13 February 1990. The inner box outlined by heavy dark lines shows the location of the Fig. 4 mesonet winds analysis. For reference the vector length corresponding to the maximum wind is also shown.

tion developed between 1500 and 1800 GMT as the surface flow veered from easterly to southeasterly. The PMM predicted flow (Fig. 7) for this time is in quite close agreement to the observed flow virtually replicating the DC's strength and position. These comparisons demonstrate not only that model correctly simulates the DC, but also that it captures the timing of DC development. Comparisons of the model's predicted surface flows with the mesonet observed surface flow at other times (not shown) are also good. It should be noted that a 6 km horizontal grid resolution was used to generate the DC circulation as shown.

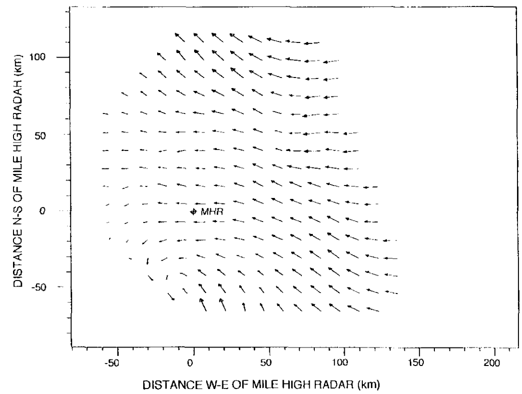

Fig. 6. As for Fig. 4 but at 1800 GMT. Note the distinct Denver cyclone circulation in the lower left part of the area about 60 km south of MHR.

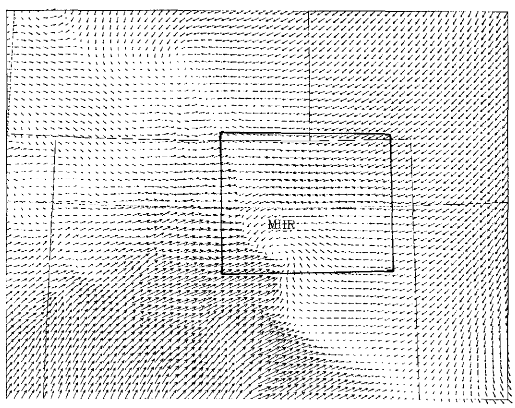

Fig. 7. As for Fig. 5, but at 1800 GMT.

With a resolution of 20 km, the circulation was much less apparent due to the inability of the model with such a grid spacing to adequately resolve the approximate 50 km scale of this circulation. Modica et al. (1994) simulated this case with a 10 km horizontal grid spacing and were successful in capturing some aspects of the observed DC circulation.

The results of the comparisons shown and discussed above indicate that the PMM has captured the mesoscale dynamical forcings of this case reasonably well especially in eastern Colorado where most of the cloud observations were made. Further evidence of this is that the vertical and horizontal distribution of cloud and horizontal distribution of precipitation predicted by the PMM is in substantial agreement with the observations. This is a good indication that the model is able to capture much of the dynamical forcing of this case because the cloud distribution is very sensitive to temperature, moisture, and vertical motion.

The observed visible image of the cloud cover over Colorado and vicinity at 1700 GMT is shown in Fig. 8; this includes a complex mixture of both high and low clouds. The major features are a large band of higher clouds running from central Utah across Wyoming into South Dakota associated with the upper jet-streak, some discontinuous cloud cover over the higher terrain in southwestern and central Colorado associated with convective activity there, and an extensive shallow cloud layer over much of eastern Colorado extending northeastward across Nebraska associated with the upslope flow and embedded fronts. It is also noteworthy that a hole in the low cloud layer is clearly visible in western Nebraska adjacent to the northeastern corner of Colorado. Therefore, the observed cloud cover is a complex composite stemming from several different dynamical forcings acting on the extant moisture distribution. In order for the model to give a similar distribution of cloud cover, it is necessary that it includes all the dynamical forcings of this situation.

In Fig. 9, we show a composite of the cloud cover predicted by the model at nearly the same time (1800 GMT on 13 February) for direct com-

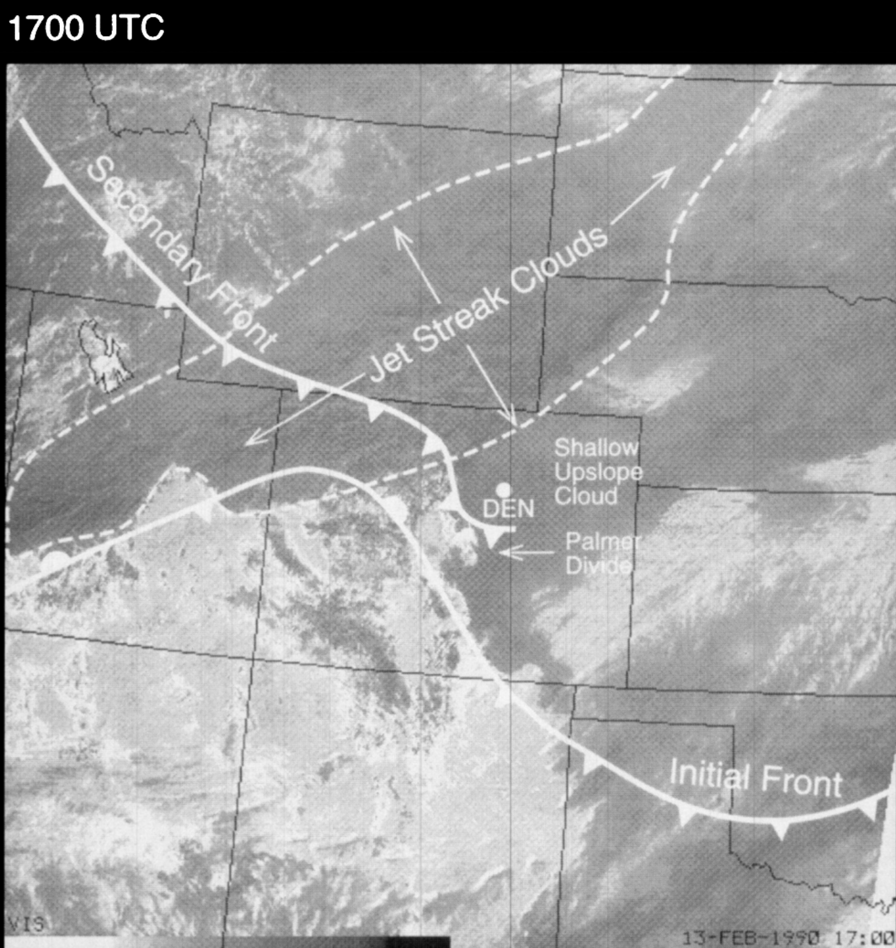

Fig. 8. Visible satellite image at 1700 GMT on 13 February 1990. Colorado is in the center of the domain. (after Rasmussen et al., 1995).

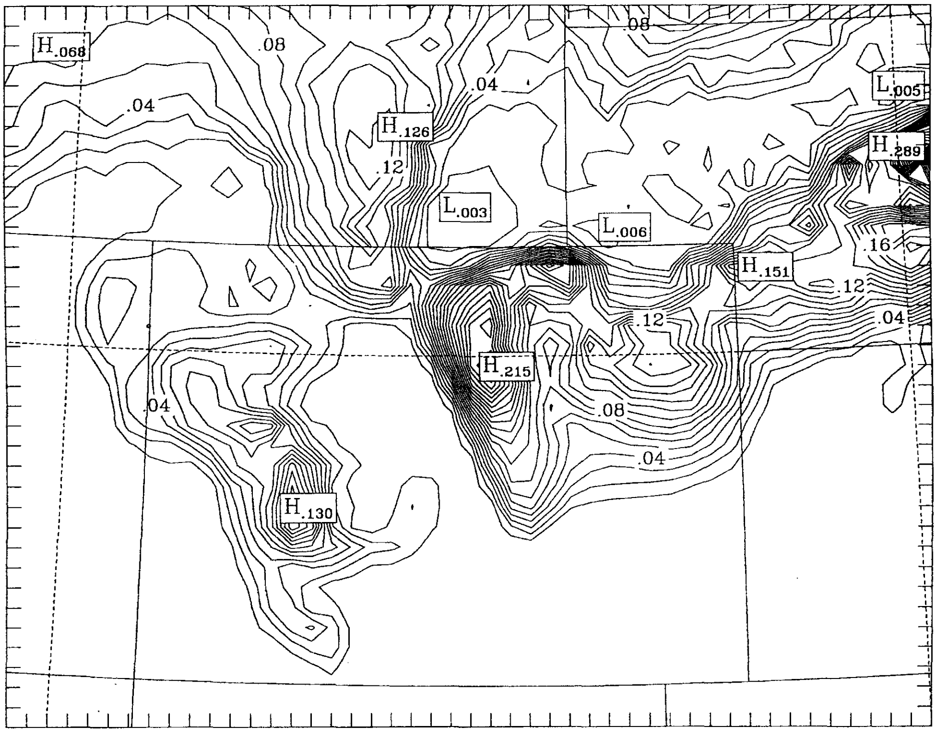

Fig. 9. Composite of PMM forecasted cloud for 1800 GMT on 13 February 1990. Units shown are mm of integrated liquid water (ILW). The mainly low and shallow clouds over eastern Colorado and Nebraska contain the most liquid water and show the largest ILW while the mainly crystalline and thicker clouds over Wyoming exhibit smaller amounts of ILW.

parison to the actual cloud cover. The distribution of the predicted cloud cover is in substantial agreement with that observed except that the observed low level cloud extends farther southward (to the New Mexico border) in eastern Colorado. While this southward extension of cloud is rather narrow in its west to east extent (about 50 to 60 km), it is nonetheless important, because there were several pilot reports of icing connected with it.

4.2. Cross-section comparisons

Aircraft observations over a two hour period from 1723 GMT to 1928 GMT were mainly confined to a south to north corridor east of the front range and will be compared to a similarly located model cross-section. Rasmussen et al. (1991) analyzed the observations on a cross section extending from approximately 100 km north of the Mile High Radar (MHR) site to 100 km south; this analysis has also been presented in Modica et al. (1994) from which Fig. 10 has been adapted. The analysis for liquid water reveals a continuous shallow cloud layer extending in altitude from about 2200 m to about 3200 m along the entire cross-section. To the north of MHR (corresponds to 0 along the lower axis in Fig. 10), the cloud base increases in height as the cloud layer becomes shallower. To the south of MHR, the highest liquid water mixing ratios (0.35 gm m^{-3}) are located in the upper half of the cloud layer while to the north of MHR liquid water amounts are less with the maximum (0.15 gm m^{-3}) located just below the cloud top. Secondary maxima of liquid water are located just above the cloud base both south and north of MHR. North of MHR, the relative minimum of liquid water amount is more extensive than to the south of MHR with values falling below 0.05 gm m^{-3}. Just above MHR,

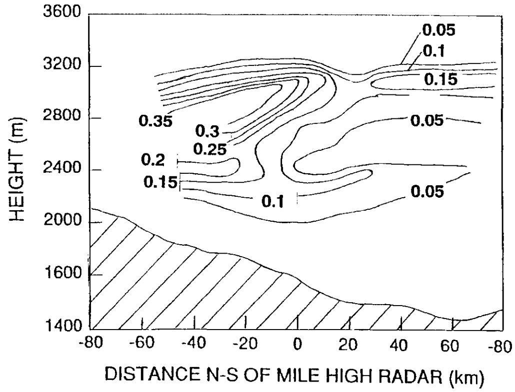

Fig. 10. South to north vertical cross section of observed cloud liquid water content in g m^{-3} derived from aircraft observations made between 1723 and 1925 GMT on 13 February 1990 (after Modica et al., 1994).

there seems to be a dividing area between the above described cloud structures.

Fig. 11 shows the liquid water values predicted by the model along this cross section. The vertical extent of the model cloud layer is quite comparable to that observed. The maximum liquid water content predicted by the model at MHR is 0.30 gm m^{-3}; this drops off somewhat to the south of MHR. To the north of MHR, the maximum value decreases to below 0.2 gm m^{-3} near the north end of the cross section. These are close to the maximum observed values. Although the liquid water is modally distributed in the vertical in the model cross section shown here, in other model cross sections located just to the east (not shown) a bimodal distribution is evident. In either case, the maximum predicted liquid water amounts are usually not located very close to the model cloud top; this is attributed to the vertical resolution used in this study. In contrast, using the high resolution 1-D Purdue Boundary Layer Model on a different case but with wind shear, Sun (1993b) showed that the liquid water reaches a maximum near the cloud top as observed. In Modica et al., the liquid water maximum along the aircraft cross-section is located uniformly in the middle of their model's cloud layer.

In order to determine how the model liquid water amounts are maintained, model condensation, precipitation production, and cloud water to cloud ice conversion rates were calculated. Of these, only three are of consequence here; the rate of ice crystal growth at the expense of cloud liquid water, P_{IDW}, was found to be very small. As shown in Fig. 12, the condensation rates along the cross section at 18Z are as high as 8×10^{-8} kg kg^{-1} s^{-1} with the highest rates located just above cloud base. At 15Z and 21Z, the condensation rates (not shown) are similar to those at 18Z except to the south of MHR at 21 Z when the location of the maximum rates rises and its value increases to 1.5×10^{-7} kg kg^{-1} s^{-1}. Depleting the liquid water are depositional growth, P_{SDEP}, and accretion of cloud water by snow, P_{SACW}. The P_{SDEP} rates along the cross section at 18 Z are shown in Fig. 13. To the north of MHR the rates are as high as 6×10^{-8} kg kg^{-1} s^{-1} but are considerably less to the south of MHR. Meanwhile, the P_{SACW} rates shown in Fig. 14 are larger; they are as high as 7×10^{-8} kg kg^{-1} s^{-1} to the north of MHR but are much less to the south of MHR. Taken together, P_{SDEP} and P_{SACW}, effectively deplete the liquid water to the north of MHR except close to the cloud top.

Rasmussen et al. (1995) note that freezing drizzle formed to the south of MHR despite maximum

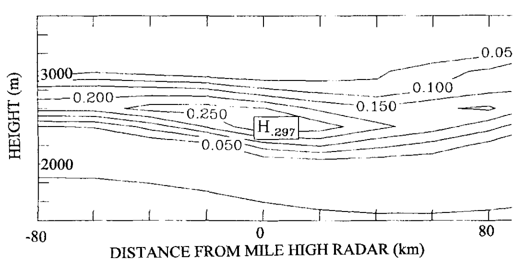

Fig. 11. South to north cross section of PMM 18-h forecast of cloud liquid water (g m^{-3}). Contour intervals are 0.05 g m^{-3}.

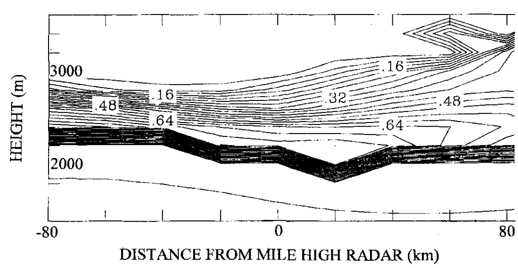

Fig. 12. Rate of liquid water production by condensation (kg kg^{-1} s^{-1} $\times 10^{-8}$) by the PMM along the aircraft observed cross section at 1800 GMT on 13 February 1990.

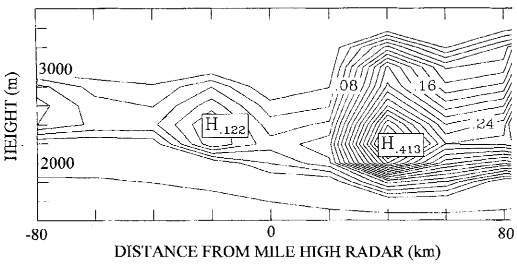

Fig. 13. Rate of PMM snow production by depositional growth of ice crystals, P_{SDEP}, (kg kg^{-1} s^{-1} $\times 10^{-8}$) along the aircraft observed cross section for 1800 GMT on 13 February 1990.

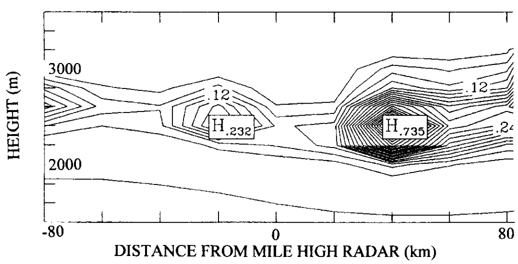

Fig. 14. Rate of PMM snow production by accretion of cloud water, P_{SACW}, (kg kg^{-1} s^{-1} $\times 10^{-8}$) along the aircraft observed cross section for 1800 GMT on 13 February 1990.

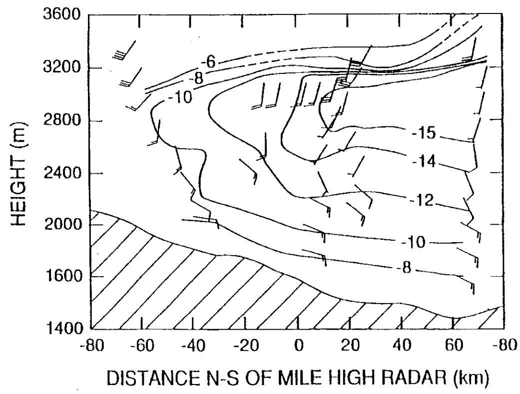

Fig. 15. South to north cross-section of temperature (°C) observed by the University of Wyoming aircraft during the time period from 1731 GMT to 1928 GMT on 13 February 1990 (after Rasmussen et al., 1995).

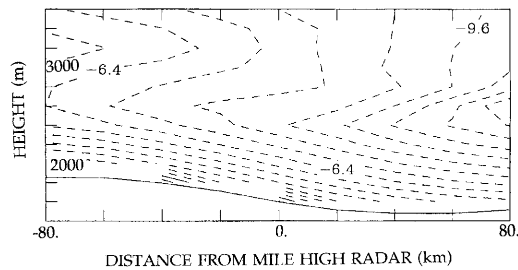

Fig. 16. Temperature (°C) predicted by the PMM along the same cross section as in Fig. 15 for 1800 GMT on 13 February 1990.

cloud water amounts that usually preclude efficient collisional growth. They suggested either a low CCN concentration or a shear induced mixing process results in sufficient numbers of 40 micron and larger drops to make collisional growth possible. The cloud parameterization used in this study does not include such a process so depletion of liquid water to the south of MHR is accomplished by PSACW and PSDEP. The fact that the model's prediction of cloud water is close to that observed there may be somewhat fortuitous because both the model's condensation and depletion rates are likely less than the actual rates.

Fig. 15 shows the observed temperatures and winds along this cross section. The coldest temperatures (−15°C) were located between 2600 and 3000 m to the north of MHR. Above this, the temperature increases from 5°C to 10°C in 100 to 200 m through a strong frontal inversion; in this same vertical interval, the wind speed increases about 15 m s^{-1} and its direction changes from east to southeast to southwest. The modeled temperatures along this cross section are shown in Fig. 16. The thermal structure is in reasonable agreement with that observed; however, because of the model's vertical resolution, the inversion is neither as strong nor as sharp as observed. The model's inversion is broadened to 400 to 600 m in contrast to the observed 100 to 200 m, hence, the upper part of the model cloud layer is warmer and dryer than the real cloud. Modica et al.'s results show a similar vertical broadening of the cloud top inversion. In addition, because of less liquid water at the model's cloud top, the intensity of the radiative flux is also greatly reduced there.

Winds in the cold air were easterly. They back with height to south and south-south west above the inversion. The predicted winds (not shown) in proximity to the ground are east to southeasterly up to 10 m s^{-1} close to the observed 7 to 8 m s^{-1}. They back with height and increase near and above the inversion in agreement with the observations although the modeled gradient of wind through the shear layer is less than was observed. In general, there is good agreement between the model and the observations along this cross-section.

4.3. *Other comparisons*

The results presented thus far demonstrate that PMM simulates many aspects of the VDS well, but there are other indirect observation sources that are useful in examining the validity of the model results such as the radiometers and pilot reports of icing. Vertically integrated values of total liquid water were derived by the dual-channel vertically pointing radiometers every 2 min throughout the VDS case. Although these measurements are incapable of revealing the vertical distribution of liquid water, they do indicate the presence and total amount of liquid water overhead, and can be readily compared to model results.

The three radiometers were located at Elbert, Platteville, and Denver as shown in Fig. 1. All three indicated appreciable liquid water at 1800 GMT: Platteville (0.25 mm), Denver (0.30 mm), and Elbert (0.35 mm). The total column amounts of liquid water predicted at this time are quite comparable at two locations: Denver (0.16 mm) and Platteville (0.14 mm); but somewhat less at Elbert (0.1 mm). Elbert is the most southerly of the radiometer sites and near the southern edge of the model cloud cover so this discrepancy is consistent with the model's not forming clouds as far south as was observed.

Another source of information are the many pilot reports of icing made during this time period. Where reports are received is a direct indication of existence of liquid water with some correlation to its amount. Where there are no reports is not necessarily an indication of absence of liquid water since low level aircraft activity tends to cluster around certain heavily populated areas such as Denver and may even be preferentially distributed along certain heavily used routes leading to or from there. Heavily used routes approach Denver from the northeast through Nebraska and from the east and southeast through Kansas. We can assume that there would have been several aircraft moving along these corridors in this time period. Another factor is aircraft altitude since transport aircraft normally fly at high altitudes well above icing hazards and ascend/descend during the first/last 100 miles or so of a flight. Other locations such as small and regional airports might have had aircraft activity that was curtailed by the known icing occurrence of this case. Thus, it is best to use the icing reports as confirmation of the existence of SLW with some correlation between the reported severity and the amount of SLW.

Most of the pilot reports of icing in the WISP domain in a three hour time period bracketing 1800 GMT on 13 February are located very close to Denver and are related to transport activity into and out of Stapleton airport. In this time span, there were a few reports well away from Denver: one report to the east of Greeley; one report to the southeast of Denver over the Palmer Divide; one report over Colorado Springs; and two reports to the southwest of Pueblo. The reported severities were generally in the moderate range indicative of significant amounts of SLW. The reported altitudes were generally at and below 10000 feet (3000 m) probably in the vicinity of the cloud top level. The distribution and severities of the reports validates the model's prediction of SLW except for the most southerly reports which were in the narrow southward extension of the cloud cover just east of the Rockies not forecast by the model. Earlier at 1301 GMT, there was an icing report in southwestern Nebraska between 5800 and 9500 feet possibly in connection with the band of liquid water predicted by the model there. There are no further reports from this vicinity indicating either the curtailment of aircraft activity or the abatement of aircraft icing conditions there.

The final comparison between the model and observations is for precipitation. Precipitation is often considered valuable in assessing the degree of success that a model has had in simulating a given situation because its occurrence and amount reflect both large and small scale forcings. There are relatively few precipitation reports available for this case so this comparison is, of necessity, qualitative in nature. Fig. 17 shows the 18-h model prediction of precipitation valid at 1800 GMT on 13 February. Fairly heavy precipitation (up to 20 mm) was predicted over the western third of Colorado; this is largely attributable to the model's cumulus parameterization. Meanwhile, wide-

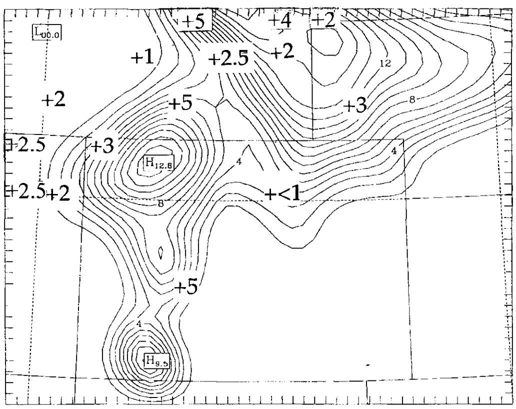

Fig. 17. 18-h prediction of precipitation (mm) starting from 0000 GMT of 13 February. Observed values from surface reporting stations are denoted by plus signs.

spread lighter stable precipitation was forecast over the eastern half of Wyoming, northern and western Nebraska, and the extreme northern part of Colorado. The average forecasted amount is slightly in excess of 5 mm with up to 10 mm predicted at a few places. The great majority of this latter precipitation is snow.

The distribution of the forecast precipitation is in good agreement with the observations (shown in bold numbers on Fig. 17) especially that part attributable to stable cloud processes. Furthermore, the model has correctly produced no precipitation over most of eastern Colorado and Kansas where little or no precipitation was observed despite the presence of cloud. There is but one precipitation report in western Colorado, 20 mm, and it is close to the forecasted amount. On the whole, the model forecasted precipitation is greater than was observed. For example, the model forecasted a large area of snow over Wyoming and Nebraska ranging from 5 to 10 mm (in melted form), as compared to the observed values of between 2 and 5 mm. There are an insufficient number of stations with which to make a definitive quantitative assessment of the model overprediction, but it does appear to be about a factor of two. Chern (1994), in using the PMM to simulate a winter cyclogenesis case over the western United States, noted that his simulated precipitation is about 1.5 times the observed amount. The excessive precipitation forecast by the model here apparently stems from use of the diagnostic technique for predicting the surface precipitation fluxes (eqs. (3) and (4)).

5. Conclusions

This study has been concerned with evaluating the capability of the PMM to simulate the conditions of the first day (13 February) of the WISP 1990 VDS case. The new PMM stable cloud parameterization was also introduced and described here. Beginning at 0000 GMT on 13 February, 1990, the PMM was used to make an 18 hour forecast of conditions in the WISP observation area. The initial conditions and time dependent lateral boundary conditions were obtained from the ECMWF analyses. Forecast fields are available from the PMM every 6 h during this period; however, we focused on the 1800 GMT PMM results since there are many observations at this time as well as many reports of moderate to severe aircraft icing.

In order to validate the capability of the PMM to simulate the large scale dynamics of this event with a reasonable degree of fidelity, we compared its results to both CLASS and mesonet observations. In addition to these favorable comparisons, the horizontal and vertical distributions of the model cloud cover are in good agreement with the observations. In terms of microphysical comparisons, the sources of discrepancies between model and observation are more likely due to the model resolution and the microphysical parameterizations. Intense turbulent mixing was observed in this case at and just above the cloud top level, but it did not extend far into the cloud layer. The model resolution of about 200 m, used here, spreads the temperature gradient over a broader vertical interval resulting in a warmer and dryer cloud than observed. Despite this, we find that the model demonstrates considerable skill in forecasting when and where the cloud forms, the resulting cloud base and cloud top, and the phase of the formed cloud. In addition, even with the vertical resolution used here, the model's cloud liquid water contents are quite comparable to those observed. These conclusions are substantiated by comparison of model forecasts with satellite, aircraft, and radiometer observations along with pilot reports of aircraft icing.

What are the prospects for applying a mesoscale model, such as the PMM, with a detailed cloud parameterization to operational forecasting of SLW? Despite being complicated by the presence of strong turbulent mixing, the results from this case were promising. It does appear that the fairly fine vertical resolutions necessary for very accurate forecasts of SLW in cases such as here are beyond current operational capabilities because of the heavy computational requirements. However, we do not know the climatology of aircraft icing situations, whether the circumstances of this case are relatively rare or common, or if the turbulent mixing in a case such as this might be amenable to parameterization.

Drop-size distribution is important to aircraft icing, but has not been considered here. Current cloud parameterization methods that include consideration of drop-size distributions require computational capabilities beyond that currently available in the operational environment. Simpler relations, of possible use for forecasting aircraft icing, are, at present, unknown.

6. Acknowledgements

We thank Tim Gilbert of the Department of Earth & Atmospheric Sciences at Purdue for his graphical expertise in the preparation of some of the figures. We also thank Richard K. Jeck and Charles Masters of the FAA Technical Center for their continuing support and advice in this work. Special thanks to Harry Orville and Fred Kopp who graciously gave a considerable amount of time in explaining cloud parameterization and the freezing of cloud water. Also special thanks to Ben Bernstein of NCAR/RAP for providing the pilot reports of aircraft icing, as well as the WISP CLASS and mesonet observations. Finally, sincere thanks to Roy Rasmussen of NCAR/RAP for providing the original of Fig. 8 for use here as well as several informative discussions. This work was supported by the FAA under Grant No. FAA-DOT 93-G-006.

REFERENCES

Chern, J.-D. 1994. *Numerical simulation of cyclogenesis over the western United States.* Ph.D. dissertation, Purdue University, 178 pp.

Federal Coordinator for Meteorological Services and Supporting Research, 1986. *National plan to improve aircraft icing forecasts.* FCM-P21-1986, Washington, DC, 24 pp.

Fletcher, N. H. 1962. *The physics of rainclouds.* Cambridge University Press, 386 pp.

Heymsfield, A. J. and Platt, C. M. R. 1984. A parameterization of the particle size spectrum of ice clouds in terms of the ambient temperature and the ice water content. *J. Atmos. Sci.* **41**, 846–855.

Hsie, E. Y., Farley, R. D. and Orville, H. D. 1980. Numerical simulation of ice-phase convective cloud seeding. *J . Appl. Meteor.* **19**, 950–977.

Koenig, L. R. 1971. Numerical modeling of ice deposition. *J. Atmos. Sci.* **28**, 226–237.

Kuo, Y.-H., Reed, R. J. and Low-nam, S. 1992. Thermal Structure and Airflow in a Model Simulation of an Occluded Marine Cyclone. *Mon. Wea. Rev.* **120**, 2280–2297.

Lin, Yuh-Lang, Farley, R. D. and Orville, H. D. 1983. Bulk parameterization of the snow field in a cloud model. *J. Appl. Meteor.* **21**, 1065–1092.

Lord, S. J., Willoughby, H. E. and Piotrowicz, J. M. 1984. Rôle of a parameterized ice-phase microphysics in an axisymmetric non-hydrostatic tropical cyclone model. *J. Atmos. Sci.* **41**, 2836–2848.

Matveev, L. T. 1984. *Cloud dynamics.* Reidel Publishing Company, Dordrecht, The Netherlands.

Modica, G. D., Heckman, S. T. and Rasmussen, R. M. 1994. An application of an explicit microphysics mesoscale model to a regional icing event. *J. Appl. Meteor.* **33**, 53–64.

Nagata, M. and Ogura, Y. 1991. A modeling study of interaction between heavy precipitation and a low-level jet over Japan in the Baiu season. *Mon Wea. Rev.* **119**, 1309–1336.

Politovich, M. K. and Bernstein, B. C. 1995. Production and depletion of supercooled liquid water in a Colorado winter storm. *J. Appl. Meteor.* **34**, 2631–2648.

Rasmussen, R. L., Murakami, M., Stossmeister, G. and Bernstein, B. C. 1991. Supercooled liquid water in Colorado front range winter storms: case study of the 1990 Valentine's day storm. Preprints, 4th Intl. Conf. Aviation Sys., Paris, *Amer. Meteor. Soc.*, 163–166.

Rasmussen, R. L., Politovich, M., Marwitz, J., Sand, W., McGinley, J. Smart, J., Pielke, R., Rutledge, S., Wesley, D., Stossmeister, G., Bernstein, B., Elmore, K., Powell, N., Westwater, E., Boba Stankov, B. and Burrows, D. 1992. Winter icing and storms project (WISP). *Bull. Amer. Meteor. Soc.* **73**, 951–974.

Rasmussen, R. M., Bernstein, B. C., Murakami, M., Stossmeister, G. and Reisner, J. 1995: The 1990 Valentine's day arctic outbreak. Part I: Mesoscale and microscale structure and evolution of a Colorado front range shallow upslope cloud. *J. Appl. Meteor.* **34**, 1481–1511.

Rutledge, S. A. and Hobbs, P. V. 1983. The mesoscale and microscale structure and organization of clouds and precipitation in midlatitude cyclones. VIII. A model for the "seeder-feeder" process in warm-frontal rainbands. *J. Atmos. Sci.* **40**, 1185–1206.

Rutledge S. A. and Hobbs, P. V. 1984. The mesoscale and microscale structure and organization of clouds and precipitation in midlatitude cyclones. (XII) A diagnostic modeling study of precipitation development in narrow cold-frontal rainbands. *J. Atmos. Sci.* **41**, 2949–2972.

Sun, W.-Y. 1980. A foward-backward time integration scheme to treat internal gravity waves. *Mon. Wea. Rev.* **108**, 402–407.

Sun, W.-Y. 1984. Numerical analysis for hydrostatic and non-hydrostatic equation of inertial-internal gravity waves. *Mon. Wea. Rev.* **112**, 259–268.

Sun, W.-Y., Chern, J. D., Wu, C.-C. and Hsu, W. R. 1991. Numerical simulation of mesoscale circulations in Taiwan and surrounding area. *Mon. Wea. Rev.* **119**, 2558–2573.

Sun, W.-Y. and Wu, C.-C. 1992. Formation and diurnal oscillation on dryline. *J. Atmos. Sci.* **49**, 1606–1619.

Sun, W.-Y. 1993a. Numerical simulation of a planetary boundary: Part I. Cloud free case. *Beitr. Phys. Atmosph.* **66**, 3–16.

Sun, W.-Y. 1993b. Numerical simulation of a planetary boundary: Part II. Cloudy case. *Beitr. Phys. Atmosph.* **66**, 17–29.

Sun, W.-Y. and Chern, J.-D. 1993. Diurnal variation of lee vortices in Taiwan and the surrounding area. *J. Atmos. Sci.* **50**, 3404–3430.

Sun, W.-Y. and Chern, J.-D. 1994. Numerical experiments of vortices in the wakes of large idealized mountains. *J. Atmos. Sci.* **51**, 191–209.

Sundqvist, H., Berge, E. and Kristjansson, J. E. 1989. Condensation and cloud parameterization studies with a mesoscale numerical weather prediction model. *Mon. Wea. Rev.* **117**, 1641–1657.

Sundqvist, H. 1993. Inclusion of ice phase of hydrometeors in cloud parameterization for mesoscale and largescale models. *Beitr. Phys. Atmosph.* **66**, 137–147.

Szoke, E. J., Weisman, M. L., Brown, J. M., Caracena, F. and Schlatter, T. W. 1984. A subsynoptic analysis of the Denver tornado of 3 June 1981. *Mon. Wea. Rev.* **112**, 790–808.

Tansey, S. F. and McCann, D. W. 1997. A preliminary evaluation of numerical model cloud liquid water and aircraft icing intensity. Preprints, *7th Conference on Aviation, range and aerospce meteorology of the AMS*, pp. 144–145.

Tao, W. K., Simpson, J. and McCumber, M. 1989. An ice-water saturation adjustment. *Mon. Wea. Rev.* **117**, 231–235.

Tripoli, G. J. and Cotton, W. R. 1981. The use of ice-liquid water potential temperature as a thermodynamic variable in deep atmospheric models. *Mon. Wea. Rev.* **109**, 1094–1102.

Wu, C.-C. and Sun, W.-Y. 1990. Diurnal oscillation of the convective boundary layer. Part 2: Cloudy atmosphere. *Terr. Atmos. Oceanic Sci.* **1**, 157–174.

Zhang, D.-L. and Gao, K. 1989. Numerical simulation of an intense squall line during 10–11 June 1985 PRE-STORM. Part II: Rear inflow, surface pressure perturbations and stratiform precipitation. *Mon. Wea. Rev.* **117**, 2067–2094.

Zhao, Q. 1993. *The incorporation and initialization of cloud water/ice in an operational forecast model.* PhD dissertation. The School of Meteorology, University of Oklahoma, Norman, OK 73072, 195 pp.